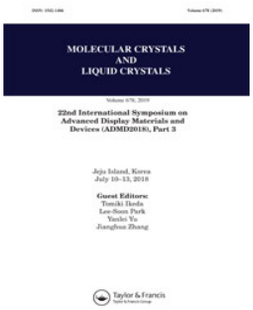

Molecular Crystals and Liquid Crystals

ISSN: 1542-1406 (Print) 1563-5287 (Online) Journal homepage: https://www.tandfonline.com/loi/gmcl20

Preparation and synthesis of carbon nanomaterials from 1-hexanol by solution plasma process with Ar/O_2 gas bubbles

Jun-Goo Shin, Choon-Sang Park, Hyun-Jin Kim, Dae Sub Kum, Eun Young Jung, Gyu Tae Bae, Hyo Jun Jang, Jae Young Kim, Byung-Gwon Cho, Bhum Jae Shin & Heung-Sik Tae

To cite this article: Jun-Goo Shin, Choon-Sang Park, Hyun-Jin Kim, Dae Sub Kum, Eun Young Jung, Gyu Tae Bae, Hyo Jun Jang, Jae Young Kim, Byung-Gwon Cho, Bhum Jae Shin & Heung-Sik Tae (2019) Preparation and synthesis of carbon nanomaterials from 1-hexanol by solution plasma process with Ar/O_2 gas bubbles, Molecular Crystals and Liquid Crystals, 678:1, 20-32, DOI: 10.1080/15421406.2019.1597524

To link to this article: https://doi.org/10.1080/15421406.2019.1597524

Published online: 29 Jul 2019.

MOLECULAR CRYSTALS AND LIQUID CRYSTALS
2019, VOL. 678, NO. 1, 20–32
https://doi.org/10.1080/15421406.2019.1597524

Preparation and synthesis of carbon nanomaterials from 1-hexanol by solution plasma process with Ar/O_2 gas bubbles

Jun-Goo Shin[a]*, Choon-Sang Park[a]*, Hyun-Jin Kim[b], Dae Sub Kum[c], Eun Young Jung[a], Gyu Tae Bae[a], Hyo Jun Jang[a], Jae Young Kim[d], Byung-Gwon Cho[e], Bhum Jae Shin[f], and Heung-Sik Tae[a]

[a]School of Electronics Engineering, College of IT Engineering, Kyungpook National University, Daegu, South Korea; [b]SEMES, Cheonan, Chungcheongnam-do, South Korea; [c]WONIK IPS, Pyeongtaek, Gyeonggi-do, South Korea; [d]Department of New Biology, Daegu Gyeongbuk Institute of Science and Technology (DGIST) Daegu, South Korea; [e]Department of Display Engineering, College of Engineering, Pukyong National University, Busan, South Korea; [f]Department of Electronics Engineering, Sejong University, Seoul, South Korea

ABSTRACT

This study presents the simple and catalyst-free methods for synthesizing carbon nanomaterials from 1-hexanol alcohol by using stable solution plasma process by varying the argon (Ar), oxygen (O_2), and Ar and O_2 mixtures plasma working gas bubble. The structural characteristics of carbon nanomaterials are measured by transmission electron microscopy, Raman spectroscopy, and X-ray diffraction. The discharge characteristics are examined based on the discharge voltage, current, and optical emission spectrometer (OES) techniques. By using the external Ar gas bubble discharge during solution plasma process, the size of carbon nanoparticle and discharge voltage are decreased compared to the no gas case and the discharge current is increased, which would be due to the increase of plasma energy and enhancement of the square of plasma-liquid contact to plasma volume. By using the external O_2 gas bubble discharge during solution plasma process, whereas, the size of carbon nanoparticle is increased compared to the no gas case and the discharge voltage and current are decreased, which would be due to the production of relatively high amounts of oxygen radicals, resulting in the flame synthesis. Raman spectra results show that the degree of graphitization of the carbon nanomaterials synthesized with external Ar 150 and O_2 50 standard cubic centimeter per minutes (sccm) mixtures gas bubble during solution plasma process is observed to be greater than that of the carbon nanomaterials synthesized with the only Ar or O_2 gas bubble. This solution plasma process by varying the plasma working gas mixtures can potentially be used for the precise nanomaterial synthesis.

KEY WORDS

Solution plasma; Gas bubble; 1-hexanol; Arc discharge; Carbon nanomaterials; Size variation

1. Introduction

During the past few decades, carbon nanomaterials have attracted extensive attentions of several researchers engaged in material science, especially for application involving

CONTACT Heung-Sik Tae hstae@ee.knu.ac.kr
*These authors contributed equally to this work.

electronics, optoelectronics, sensing, imaging, medical field, and future display [1–7]. Among the various structure forms of carbon nanomaterials, carbon nanospheres have been recognized as a novel class of carbon structure with unique characteristics, such as high strength, light weight, and high thermal resistance. Solution plasma process (SPP) has been accepted as a new technology to synthesize carbon nanomaterials due to its intrinsic merits, such as catalyst-free, low cost, simple implementation, and available operating under ambient condition. SPP is new useful and simple synthesis method of carbon materials, because this plasma in solution can provide rapid reactions due to the reactive chemical species [8–15]. Nonetheless, the activated particles produced by most SPP methods without any plasma working gas bubble, including photons, electrons, ions, and radicals, have not sufficient energy to induce precise chemical reactions and to control the size of nanomaterials more precisely, which inherently results the use of plasma with unstable discharge in liquid condition.

Recently, the carbon nanomaterials prepared by solution plasma process without any plasma working gas bubble have been widely used in optoelectronic devices because carbon materials can reduce the injection barrier between anode and hole transport layer in organic or polymer light emitting devices (OLED or PLED) [16]. However, the interactions between the use of the plasma working gas in solution plasma process and the synthesis of carbon nanomaterials have not yet been studied in detail.

Accordingly, this study investigates the one-step with high-speed and catalyst-free method for the synthesis of carbon nanomaterials from 1-hexanol in a simple solution plasma source with plasma working gas variation. In order to produce stable plasma with high plasma density and to control the size of carbon nanomaterials, we use an external plasma working gas between two electrodes to decrease the discharge voltage with unnecessary current and to minimize the unstable discharge in SPP reactor. Using of external plasma working gas bubble between two electrodes inhibits development of the ionization instability in plasma of the discharge [17–23], provides high uniformity of parameters on the plasma-liquid boundary in real plasma-chemical process.

2. Experiment

Figure 1 shows a schematic diagram of the solution plasma reactor and measurement setup with an external plasma working gas system for synthesizing carbon nanomaterials employed. The solution plasma reactor consisted of the vertical cylindrical glass test-tube (outer diameter (O.D.) = 20 mm, inner diameter (I.D.) = 18 mm, and height = 150 mm) supplied by one glass inlet plasma working gas pipe and two tungsten electrodes. The reactor was filled by the 1-hexanol (Yakuri Pure Chemicals Co., Ltd, 99.0%) solution; the argon (Ar) and oxygen (O_2) gases entered into the reactor through the glass inlet gas pipe (O.D. = 2 mm and I.D. = 1 mm) system. The Ar and O_2 flow rates were varied from 0 to 200 standard cubic centimeter per minutes (sccm) and from 0 to 200 sccm, respectively. The detailed gas mixtures are listed in Table I. Two tungsten wires with a diameter of 0.5 mm, covered with polytetrafluoroethylene (PTFE) and a glass tube, were applied as the electrodes, one on each side of the solution plasma reactor. The gap between the two electrodes was set to 1 mm in the solution. It formed a bubble-type flow gas channel with a surrounding liquid wall in the volume between

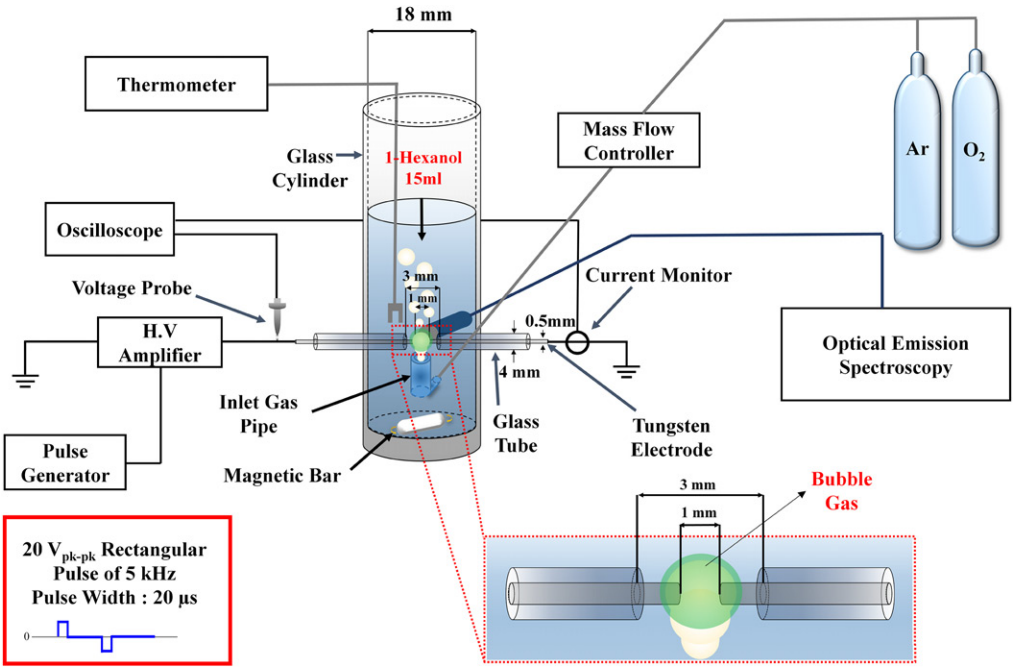

Figure 1. Schematic diagram of solution plasma reactor and measurement setup employed in this study.

Table 1. Plasma working gas conditions employed in this study.

Plasma Working Gas Conditions		
No Gas	Ar 100 sccm	Ar 200 sccm
O_2 100 sccm	O_2 150 sccm	O_2 200 sccm
Ar 150 sccm + O_2 50 sccm	Ar 100 sccm + O_2 100 sccm	Ar 50 sccm + O_2 150 sccm

Table 2. Power sources to generate bipolar pulse for solution plasma reactor.

Equipment	Manufacturer	Model	Specifications
High-voltage amplifier	Trek, Inc.	20/20C-HS	Gain: 2000 V/V Slew rate: 800 V/μs
Pulse generator	Tektronix, Inc.	AFG-3102	Amplitude: 20 mVp-p to 20 Vp-p Rise time: $\leq$ 5 ns

immersed two electrodes where an electrical breakdown occurred. The solution was mixed by a magnetic stirring bar with a rotational speed of 1000 rpm in the reactor to reduce the particle aggregation. The discharge was powered by the function generator (Tektronix AFG-3102) and bipolar pulsed high-voltage amplifier (Trek Inc. 20/20C-HS). The bipolar pulse with 5 kHz of a frequency was used and applied voltages of peak to peak value were employed 10 kV between two electrodes. The detailed specifications of power sources for solution plasma process (SPP) are listed in Table II. A high-voltage probe (Tektronix P6015A) and current probe (Pearson 4100) were connected between the power source via an inverter circuit and oscilloscope (LeCroy, WaveRunner 64Xi) to measure the applied voltage, discharge voltage, and discharge current. An optical emission spectrometer (OES, Ocean Optics, USB-4000 UV-Vis) was employed to analyze the optical intensity and spectra of various reactive species in the solution plasma

for estimating the variations in the plasma energy states [24, 25]. All the photographs of the devices, plasma, and synthesized carbon nanomaterials in solution were taken using a DSLR camera (Nikon D56300) with a Macro 1:1 lens (Tamron SP AF 90mm F2.8 Di). To investigate the solution temperature during SPP in 1-hexanol alcohol, thermometer (HANYOUNG NUX, D55) was used. Temperature was measured by placing thermometer probe 1 cm above the two electrodes in 1-hexanol alcohol. To analyze sizes of the synthesized carbon nanomaterials, the transmission electron microscopy (TEM) images were taken with a Titan G2 ChemiSTEM Cs Probe (FEI Company) transmission electron microscope. TEM samples of carbon nanomaterials were prepared by depositing 5-μL solution on carbon-coated copper grids and dried in air. Raman scattering was performed on a Renishaw (inVia reflex) Raman spectroscopy using the second harmonic (532 nm) to analyze graphitization and structure properties of the synthesized carbon nanomaterials. X-ray diffraction (XRD) was obtained from XRD system (Bruker D6 Discover, Billerica, MA, USA) at 40 kV and 40 mA using Cu-kα ($\lambda = 1.5406$ Å) as the radiation source to determine crystallinity of synthesized carbon nanoparticles. The scanning angle 2θ was varied in the range of 15-70°.

3. Result and discussion

Figure 2 shows the plasma images and solution color changes of the 1-hexanol in the SPP under the various process times. The colors of the solutions for all cases changed from transparent to dark or yellowish-brown color during the process time, indicating that some particles were synthesized from the 1-hexanol alcohol solutions. As the

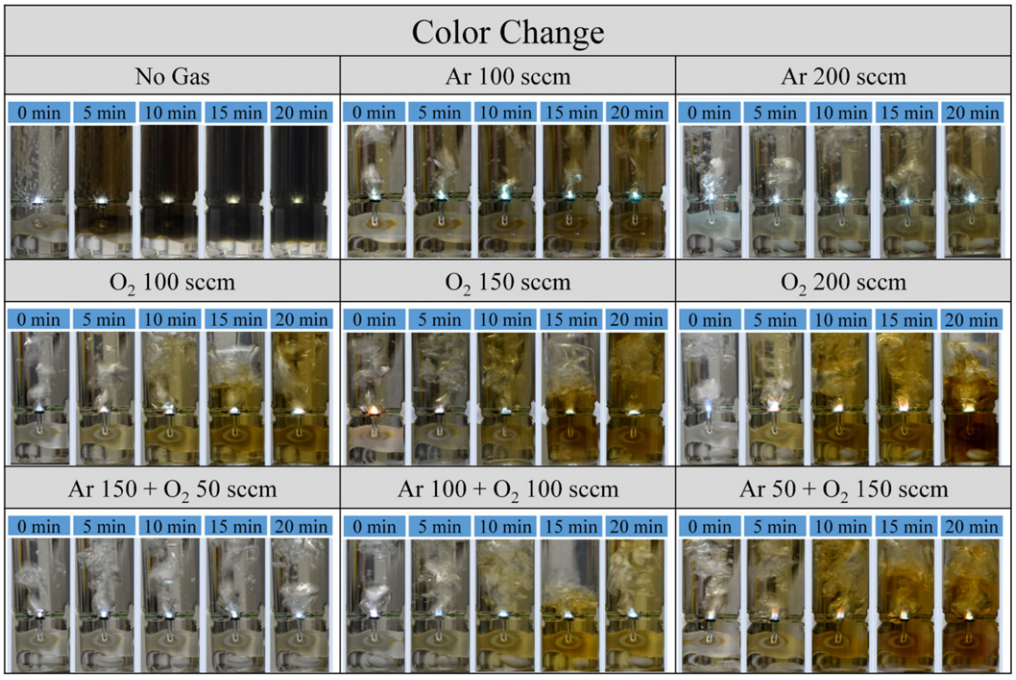

Figure 2. Changes in solution colors with plasma images of 1-hexanol alcohol under various plasma working gas conditions under 20-min plasma synthesis times via solution plasma process (SPP).

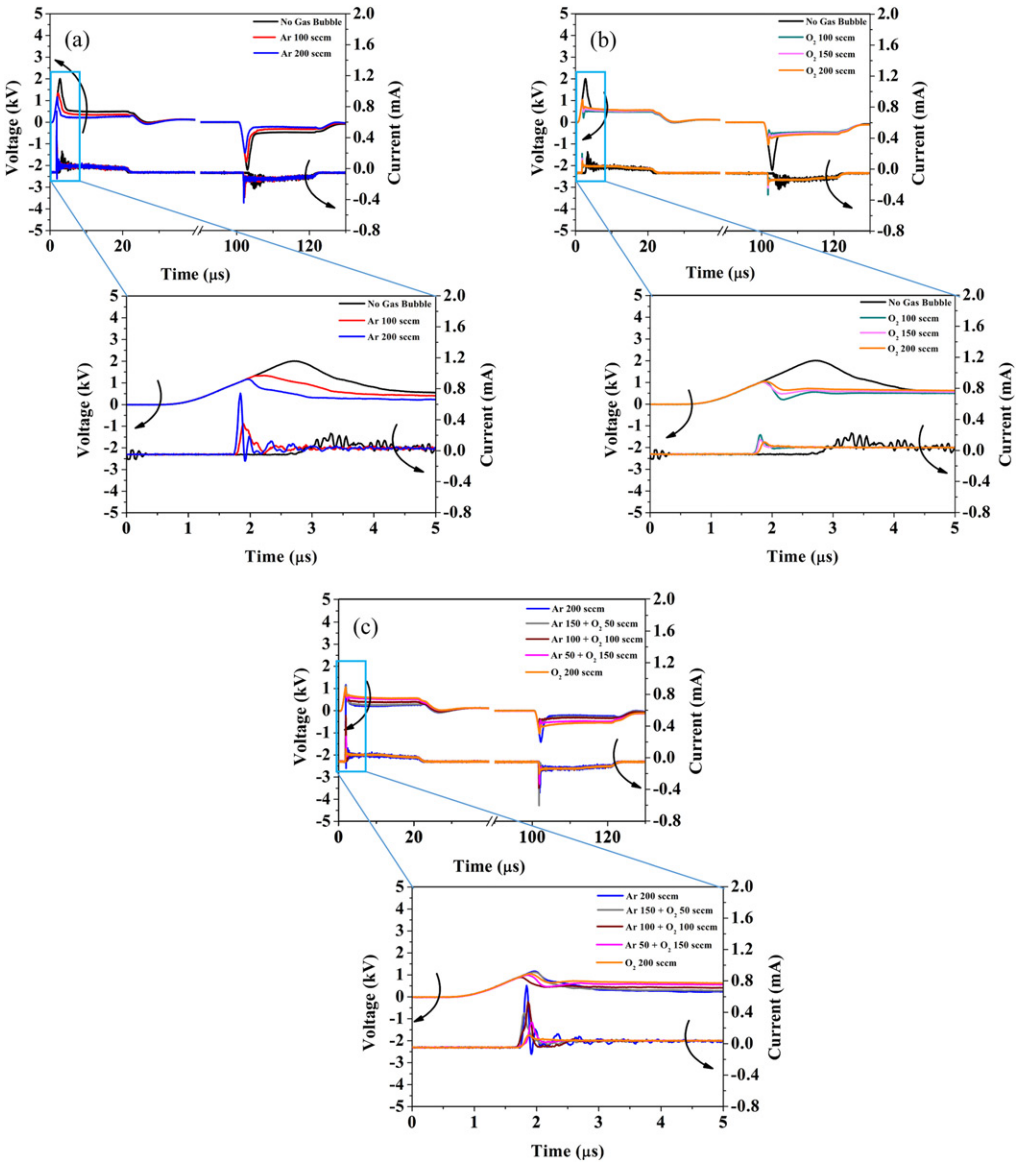

Figure 3. Measured discharge voltages and currents during plasma synthesis in 1-hexanol alcohol via SPP under various (a) Ar, (b) O_2, and (c) $Ar + O_2$ mixtures gas flow rates, respectively.

external Ar or O_2 gas flow rates were increased in the range from 0 (No gas case) to 200 sccm, as shown in Figure 2, the color changes of the 1-hexanol during SPP were slowly changed, which means that the external plasma working gas would play a different role in synthesizing the carbon nanomaterials, especially the synthesis rate and size of carbon nanomaterials.

Figure 3 shows the measured discharge voltages and the discharge currents during the plasma synthesis in 1-hexanol alcohol via SPP under various Ar, O_2, and $Ar + O_2$ mixtures gas flow rates. As the Ar gas flow rates during SPP were increased in the range from 0 to 200 sccm in Figure 3 (a), the discharge voltage was decreased compared to

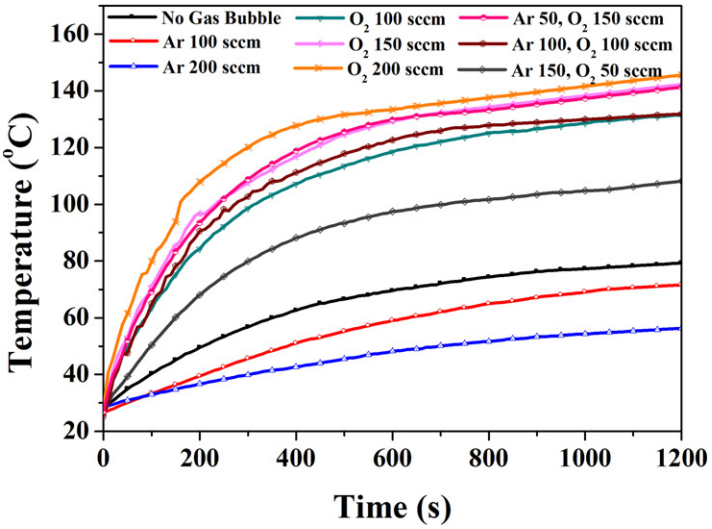

Figure 4. Variations of solution temperature curves in 1-hexanol alcohol during 20-min using SPP under various plasma working gas conditions.

the no gas case and the discharge current was increased, which would be due to the increase of ionization of gas. In addition, when applying the external Ar gas bubble in SPP reactor, the current spikes were decreased, so that the resulting stable discharge contributed to reducing unnecessary current spikes during plasma synthesis of carbon nanomaterials from the 1-hexanol. Whereas, as the O_2 gas flow rates were increased in the range from 0 to 200 sccm in Figure 3 (b), the discharge voltage and current were almost same, which would be due to the production of the flame synthesis with high temperature. On the other hands, in $Ar + O_2$ mixtures gas cases from Figure 3 (c), when the Ar flow rates at 150 sccm and O_2 flow rates at 50 sccm during SPP was adopted, the current spikes were observed to be extremely decreased without any flame discharge and voltage drop [26], thereby producing the more stable discharge.

Figure 4 shows the variations of solution temperature curves during SPP for 20-min in 1-hexanol alcohol under various plasma working gas conditions. As the Ar gas flow rates during SPP were increased in the range from 0 to 200 sccm, the solution temperatures after 20-min were decreased from 79.3 to 56.3°, which would be due to the reduction of unnecessary current spikes and the generation of stable discharge during plasma synthesis of carbon nanomaterials from the 1-hexanol. Whereas, as the O_2 gas flow rates during SPP were increased in the range from 0 to 200 sccm, the solution temperatures after 20-min were extremely increased from 79.3 to 145.6°, which would be due to the production of the flame synthesis with high temperature. Especially, when the O_2 flow rate at 200 sccm during SPP was adopted, the variation of solution temperature was observed to be increased significantly and rapidly during 6-min [27–30]. However, when the Ar flow rates at 150 sccm and O_2 flow rates at 50 sccm during SPP was adopted, the solution temperature was observed to be slightly increased without any flame discharge and unstable discharge.

Figure 5 shows the optical emission spectra measured between two electrodes of the solution plasma reactor during the plasma synthesis in 1-hexanol alcohol via SPP under

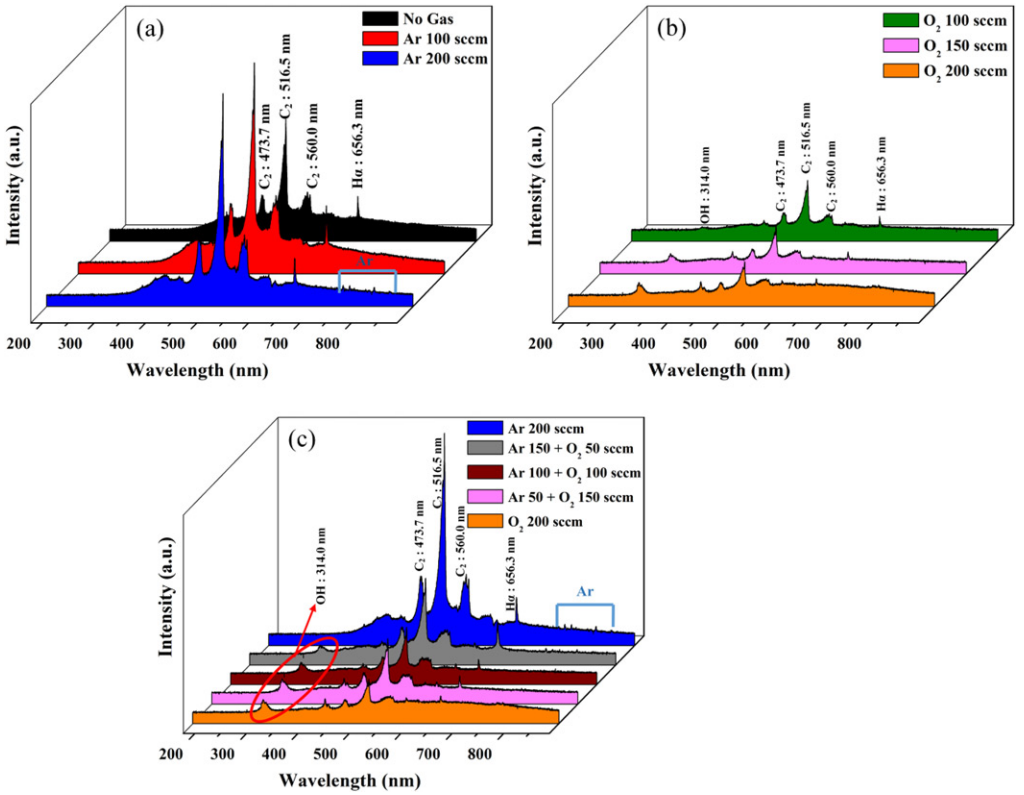

Figure 5. Optical emission spectra (OES) measured between two electrode of solution plasma reactor during plasma synthesis in 1-hexanol alcohol via SPP under various (a) Ar, (b) O_2, and (c) $Ar + O_2$ mixtures gas flow rates, respectively.

various Ar, O_2, and $Ar + O_2$ mixtures gas flow rates. OES was performed to elucidate the relation between the states of plasma and the obtained products [9, 10, 12]. During the discharge, active species including OH (314.0 nm), Hα (656.3 nm), various C_2 (473.7, 516.5, and 560.0 nm) peaks were generated during molecule dissociation, atomic and molecular excitation. As shown in Figure 5 (a), as the Ar gas flow rates during SPP were increased in the range from 0 to 200 sccm, the peak intensities of Hα were almost same. However, the various C_2 peaks of active species were observed to be increased, which would be due to the increase of plasma energy. Meanwhile, C_2 molecules were generated at the interface between the plasma and solution. In addition, when applying the externally supplied Ar gas bubble in SPP reactor, the Ar peak were newly observed. Whereas, as the O_2 gas flow rates were increased in the range from 0 to 200 sccm in Figure 5 (b), the various C_2 and Hα peaks of active species were observed to be decreased and OH peaks were observed to be increased, which would be due to the production of the flame synthesis with high temperature. On the other hands, in $Ar + O_2$ mixtures gas cases from Figure 5 (c), when the Ar flow rates at 150 sccm and O_2 flow rates at 50 sccm during SPP was adopted, the active species including OH, Hα, various C_2 peaks were observed to be increased compared to another mixtures gas cases, except for the Ar 200 sccm case. These OES data show that the SPP using the only Ar gas or the Ar flow rates at 150 sccm and O_2 flow rates at 50 sccm could be suitable for a

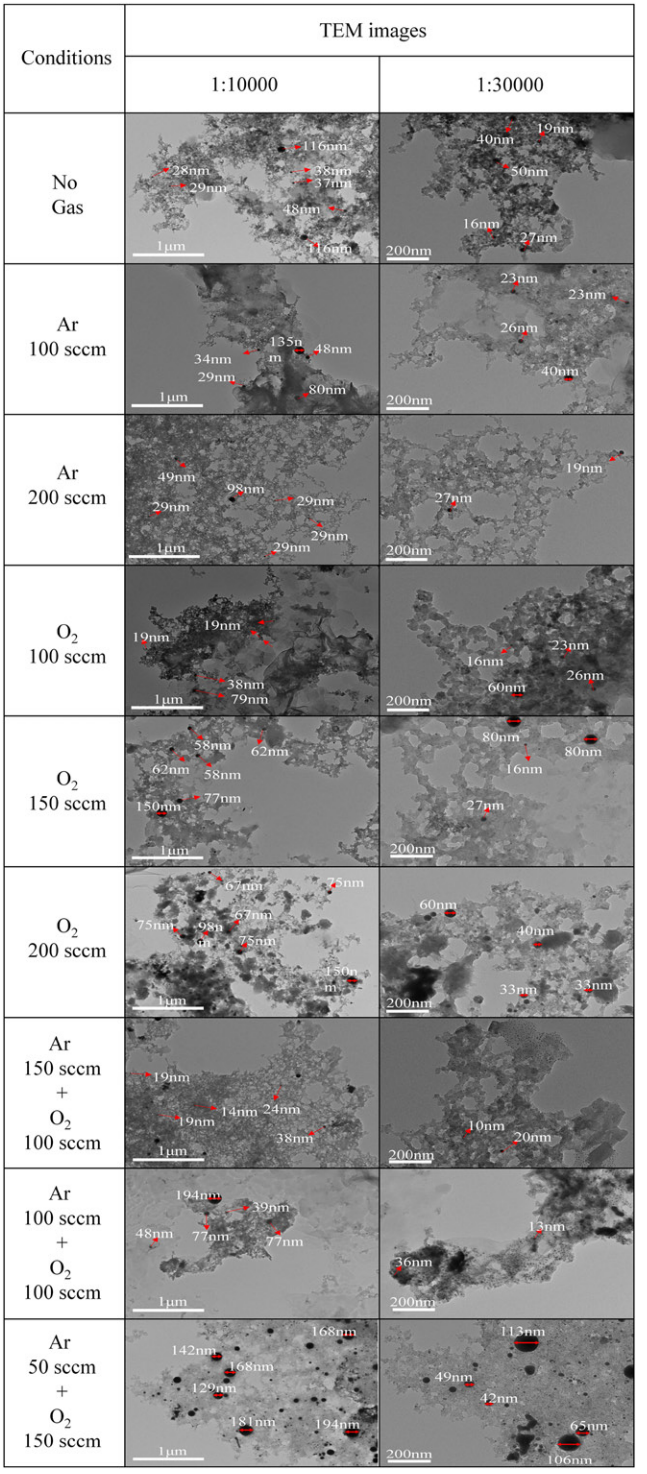

Figure 6. Transmission electron microscopy (TEM) images of synthesized carbon nanoparticles from 1-hexanol alcohol after 20-min plasma synthesis prepared via SPP under various plasma working gas conditions.

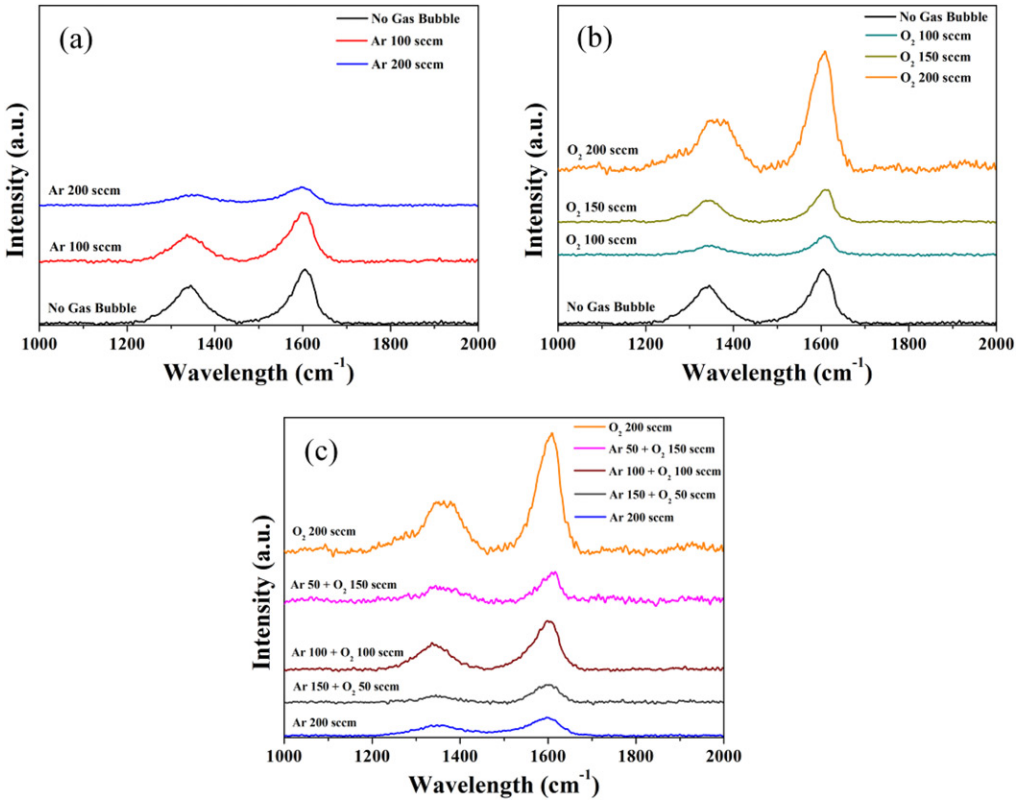

Figure 7. Raman spectra of carbon nanoparticles after 20-min plasma synthesis of nanocarbons from 1-hexanol alcohol via SPP under various (a) Ar, (b) O_2, and (c) $Ar + O_2$ mixtures gas flow rates, respectively.

sufficient fragmentation of the 1-hexanol solution and an efficient synthesis of carbon nanomaterials.

The TEM was employed to analyze the size of carbon nanomaterials. The same has been focused for a higher magnification using a high-resolution TEM (HR-TEM). Figure 6 shows TEM images of the synthesized carbon nanoparticles from 1-hexanol alcohol after the 20-min plasma synthesis prepared via SPP under various plasma working gas conditions. In all cases, the products contained only the spherical nano-size carbon particles. As the Ar gas flow rates were increased, the size of carbon nanoparticles was decreased compared to the no gas case, which would be due to the increase of ionization of gas and enhancement of the square of plasma-liquid contact to plasm volume. Whereas, as the O_2 gas flow rates were increased, the size of carbon nanoparticles was increased, which would be due to the production of relatively high amounts of oxygen radicals, resulting in the flame synthesis. Especially, in $Ar + O_2$ mixtures gas cases, when the Ar flow rates at 150 sccm and O_2 flow rates at 50 sccm during SPP was adopted, the spherical carbon nanoparticles had very small size and their diameters been ranged from 10 to 20 nm.

We served Raman scattering technique to confirm the structural ordering of carbon and graphitic materials. Figure 7 shows Raman spectra of the carbon nanoparticles after the 20-min plasma synthesis of solution plasma reactor from 1-hexanol alcohol via SPP

Table 3. I_D/I_G ratio for obtained Raman spectra of carbon particles under various plasma working gas conditions after 20-min plasma synthesis from 1-hexanol alcohol via solution plasma process.

Conditions	I_D/I_G
No gas bubble	0.89
Ar 100 sccm	0.64
Ar 200 sccm	0.74
O_2 100 sccm	0.71
O_2 150 sccm	0.92
O_2 200 sccm	0.72
Ar 150 sccm + O_2 50 sccm	0.47
Ar 100 sccm + O_2 100 sccm	0.64
Ar 50 sccm + O_2 150 sccm	0.90

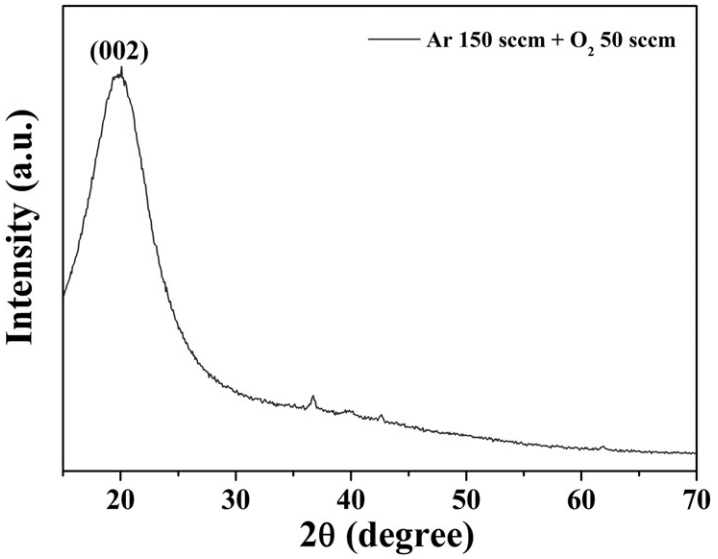

Figure 8. X-ray diffraction (XRD) pattern of synthesized carbon nanoparticles from 1-hexanol alcohol after 20-min plasma synthesis prepared via SPP under Ar 150 sccm + O_2 50 sccm mixtures gas flow condition.

under various Ar, O_2, and Ar + O_2 mixtures gas flow rates. The Raman spectrum wavelength ranges from 1000 to 2000 cm^{-1}. Raman spectrum strongly shows broadened peaks with high similarity to associated stacking disorder and defects in the carbon layer structure around 1350 cm^{-1} contributing to D band. The narrow band at 1600 cm^{-1} represents the E_{2g} mode contributing to the first order graphitized zone in G band. The ratio of D and G band intensities (I_D/I_G) indicates the degree of graphitization and crystallinity. For example, the I_D/I_G ratio of the carbon nanomaterials is 0.89, which reveals that the carbon nanomaterials are partially deformed and poorly graphitized. Table III contains the determined I_D/I_G ratios for all samples calculated from intensity of Figure 7. As shown in Table III and Figure 7, when applying the external Ar or O_2 gas bubble only in SPP reactor, the I_D/I_G ratios were slightly decreased compared to the no gas case. Whereas, when the Ar flow rates at 150 sccm and O_2 flow rates at 50 sccm during SPP was adopted, I_D/I_G ratios were considerably decreased, meaning that the degree of graphitization of the nanocarbon materials were enhanced.

The XRD pattern of synthesized carbon nanoparticles from 1-hexanol alcohol after 20-min plasma synthesis prepared via SPP under Ar 150 sccm + O_2 50 sccm mixtures gas flow condition is shown in Fig. 8. It consists of one clear reflection at 20°2θ angle and another shallow reflection between 36 and 50° 2θ angle. The characteristic peak of graphite in carbon nanomaterial was observed in the strong and broad (002) reflection at 20° 2θ angle. The broaden peak can be an indication of a widespread disordering of the structure because of the small size in carbon nanoparticles as observed in the TEM images of Fig. 6. The XRD pattern also shows a shallow reflection between 36 and 50° 2θ angle, this may be attributed to the disordered structure of the graphene rings within the carbon nanoparticles [31–35].

Consequently, these experimental results confirm that the SPP device with the Ar gas and mixtures gas system can control the size and degree of graphitization of carbon nanoparticles with stable discharge. Furthermore, we expect that this advanced solution plasma reactor with external gas bubble system and catalyst-free method will lead to a breakthrough in the precise control of carbon nanomaterials.

4. Conclusions

In summary, the novel solution plasma reactor employing the external gas bubble inlet system is proposed and investigated. Carbon nanomaterials have been successfully prepared using SPP by varying the Ar, O_2, and Ar and O_2 mixtures plasma working gas bubble. The advanced solution plasma reactor can produce a stable discharge by reducing the current spikes thanks to the use of external Ar gas. The results show that the I_D/I_G ratios are considerably decreased when adopting the Ar flow rates at 150 sccm and O_2 flow rates at 50 sccm during SPP. In all cases, the products contained only the spherical nano-size carbon particles. As the Ar gas flow rates are increased, the size of carbon nanoparticles is decreased compared to the no gas case, which would be due to the increase of plasma energy and ionization of gas. Whereas, as the O_2 gas flow rates are increased, the size of carbon nanoparticles is increased. Especially, the spherical carbon nanoparticles have very small size and their diameters ranged from 10 to 20 nm when adopting the Ar flow rates at 150 sccm and O_2 flow rates at 50 sccm during SPP. It has been found that the external gas bubble is the key factor which controls the plasma energy, size, and degree of graphitization of carbon nanomaterials synthesized from 1-hexanol. It is expected that our carbon nanomaterials can provide a unique advantage for optoelectronics, electrochemical, molecular electronics, future display, and bio-nanotechnology applications.

Acknowledgement

This work was supported by the National Research Foundation of Korea (NRF) grant funded by the Korea government (MOE) (No. 2017R1A4A1015565) to the government (MOE) (No. 2016R1D1A1B03933162) and the Korea government (MOE) (No. 2018R1D1A1B07046640).

References

[1] He, H., Pham-Huy, L. A., Dramou, P., Xiao, D., Zuo, P., & Pham-Huy, C. (2013). *Bio Med Res. Int.*, *2013*, 1.

[2] Bansal, M., Srivastava, R., Lal, C., Kamalasanan, M.N., & Tanwar, L. S. (2009). *Nanoscale*, *1*, 317.
[3] Zou, J., Zhang, K., Zhao, Y., Wang, Y., Pillai, S. K. R., Demir, H. V., Sun, X., Chan-Park, M. B., & Zhang, Q., *(*2015*). Sci. Rep.*, *5*, 1.
[4] Zaporotskova, I. V., Boroznona, N. P., Parkhomenko, Y. N., & Kozhitov, L. V. (2016). *Modern Electronic Materials*, *2*, 95.
[5] Zhang, X., Zhang, Y., Wang, Y., Kalytchuk, S., Kershaw, S. V., Wang, Y., Wang, P., Zhang, T., Zhao, Y., Zhang, H., Cui, T., Wang, Y., Zhao, J., Yu, W. W., & Rogach, A. L. (2013). *ACS NANO*, *7*, 11234.
[6] Bhunia, S. K., Saha, A., Maity, A. R., Ray, S. C., & Jana, N. R. (2013). *Sci. Rep*, *3*, 1.
[7] Chen, G., Huang, J., Yu, J., Xu, H., Bai, H., & Hu, G. (2015). *Mat. Res. Express*, *2*, 095006.
[8] David, I. G., Popa, D.-E., & Buleandra, M. (2017). *J. Anal. Methods Chem.*, *2017*, 1.
[9] Li, O. L., Kang, J., Urashima, K., & Saito, N. (2012). *International Journal of Plasma Environmental Science & Technology*, *7*, 31.
[10] Morishita, T., Ueno, T., Panomsuwan, G., Hieda, J., Yoshida, A., Bratescu, M. A., & Saito, N. (2016). *Sci. Rep*, *6*, 1.
[11] Veremii, I. P., Chernyak, V. Y., Naumov, V. V., Yukhymenko, V. V., & Dudnyk, N. V. (2006). *Probl. Atom. Sci. Tech.*, 12, 216.
[12] Kang, J., Li, O. L., & Saito, N. (2013). *Carbon*, *60*, 292.
[13] Richmonds, C., & Sankaran, R. M. (2008). *Appl. Phys. Lett.*, *93*, 131501.
[14] Pootawang, P., Saito, N., Takai, O., & Lee, S.-Y. (2012). *Nanotechnology*, *23*, 395602.
[15] Kim, H.-J., Shin, J.-G., Park, C.-S., Kum, D.-S., Shin, B.-J., Kim, J.-Y., Park, H.-D., Choi, M., & Tae, H.-S. (2018). *Materials*, *11*, 891.
[16] Zhang, R.-C, Sun, D., Zhang, R., Lin, W.-F., Macias-Montero, M., Patel, J., Askari, S., MacDonald, C., Mariotti, D., & Maguire, P. (2017). *Sci. Rep.*, *7*, 1.
[17] Sommers, B. S., & Foster, J. E. (2014). *Plasma Sources Sci. Technol.*, *23*, 015020.
[18] Hamdan, A., & Cha, M. S., (2015). *J. Phys. D*, *48*, 405206.
[19] Foster, J., Sommers, B. S., Gucker, S. N., Blankson, I. M., & Adamovsky, G. (2012). *IEEE T. Plasma Sci.*, *40*, 1311.
[20] Tian, W., Tachibana, K., & Kushner, M. J. (2014). *J. Phys. D*, *47*, 055202.
[21] Hamdan, A., & Cha, M. S., (2016). *J. Phys. D*, *49*, 245203.
[22] Tu, Y., Xia H., Yang, Y., & Lu, X. (2016). *Phys. Plasmas*, *23*, 013507.
[23] Kum, D. S., Park, C.-S., Kim, H. J., Shin, J.-G., Kim, D. H., Kim, D., Bae, G. T., Kim, J. Y., Cho, B. K., Shin, B. J., Lee, D. H., Chien, S.-I., & Tae, H. S. (2018). *Mol. Cryst. Liq. Cryst.*, *663*, 115.
[24] Park, C.-S., Kim, D. Y., Kim, D. H., Lee, H.-K., Shin, B. J., & Tae, H.-S. (2017). *Appl. Phys. Lett*, *110*, 033502.
[25] Kim, D. H., Park, C.-S., Kim, W. H., Shin, B. J., Hong, J. G., Park, T. S., Seo, J. H., & Tae, H.-S. (2017). *Phys. Plasmas*, *24*, 023506.
[26] Bruggeman, P. J., Kushiner, M. J., Locke, B. R., Gardeniers, J. G. E., Graham, W. G. Graves, D. B., Hofman-Caris, R. C. H. M., Maric, D., Reid, J. P., Ceriani, E., Rivas, D. F., Foster, J. E., Garrick, S. C., Gorbanev, Y., Hamaguchi, S., Lza, F., Jablonowski, H., Klimova, E., Kolb, J., Krcma, F., Lukes, P., Machala, Z., Marinov, I., Mariotti, D., Thagard, M, S., Minakata, D., Neyts, E. C., Pawlat, J., petrovic, Z. L., Pflieger, R., Reuter, S., Schram, D. C., Schroter, S., Shiraiwa, M., Tarabova, B., Tsai, P. A., Verlet, J. R. R., Woedtke, T. von, Wilson, K. R., Yasui, K., & Zvereva, G. (2016), *Plasma Source Sci. Technol*, *25*, 053002.
[27] Woo, S. K., Hong, Y. T., & Kwon, O. C. (2009), *Carbon*, *47*, 912–916.
[28] Chong, C. T., Tan, W. H., Lee, S. L., Chong,W. W. F., Lam, S. S., & Valera-Medina, A. (2017), *Mater. Chem. Phys.*, *197*, 246–255.
[29] Bhattacharjya, D., Park, H.-Y., Kim, M.-S., Choi, H.-S., & Inamdar, S. N. (2013), *Langmuir*, *30*, 318–324.
[30] Yuan, L., Saito, K., Hu, W., & Chen, Z. (2001), *Chem. Phys. Lett.*, *346*, 23–28.

[31] Dhand, V., Prasad, J. S., Rhee, K. Y., & Anjaneyulu, Y. (2013), *J. Ind. Eng. Chem.*, *19*, 944–949.
[32] Dhand, V., Prasad, J. S., Rao, M. V., & Bharadwaj, S., Anjaneyulu, Y., Jain, P. K. (2013), *Mater. Sci. Eng. C*, *33*, 758–762.
[33] Han, F.-D., Yao, B., & Bai, Y.-J. (2011), *J. Phys. Chem. C*, *115*, 8923–8927.
[34] Penki, T. R., Shanmughasundaram, D., Kishore, B., & Munichandraiah, N. (2014), *Adv. Mat. Lett.*, *5*, 184–190.
[35] Singh, B., Sharma, A., Sharma, A., & Dhiman, A. (2017), *American Journal of Drug Delivery and Therapeutics*, *4*, 1–9.